Hindawi
Journal of Nanomaterials
Volume 2022, Article ID 6358852, 10 pages
https://doi.org/10.1155/2022/6358852

Research Article

Fabrication of High-Performance $MgCoO_2$/PEDOT:PSS@Nickel Foam Anode for Bioelectricity Generation by Microbial Fuel Cells

Brahmari H. Shetty,[1] Ashok K. Sundramoorthy,[2] Jayshree Annamalai,[3] Preethika Murugan,[2] Raji Atchudan,[4] Sandeep Arya,[5] Asma A. Alothman,[6] and Mohamed Ouladsmane[6]

[1]*Department of Physics and Nanotechnology, SRM Institute of Science and Technology, Kattankulathur, 603203 Tamil Nadu, India*
[2]*Centre for Nano-Biosensors, Department of Prosthodontics, Saveetha Dental College and Hospitals, Saveetha Institute of Medical and Technical Sciences, Poonamallee High Road, Velappanchavadi, Chennai, 600 077 Tamil Nadu, India*
[3]*Department of Biotechnology, SRM Institute of Science and Technology, Kattankulathur, 603203 Tamil Nadu, India*
[4]*School of Chemical Engineering, Yeungnam University, Gyeongsan 38541, Republic of Korea*
[5]*Department of Physics, University of Jammu, Jammu, And Kashmir, 180006, Jammu, India*
[6]*Department of Chemistry, College of Science, King Saud University, Riyadh 11451, Saudi Arabia*

Correspondence should be addressed to Ashok K. Sundramoorthy; ashok.sundramoorthy@gmail.com

Received 9 April 2022; Revised 21 July 2022; Accepted 23 August 2022; Published 5 September 2022

Academic Editor: S Manigandan

We report the fabrication of cost-effective, biocompatible, and high-performance anode made of nickel foam (NF) modified with magnesium cobalt oxide ($MgCoO_2$) and poly(3,4-ethylenedioxythiophene) polystyrene sulfonate (PEDOT:PSS) as active components. Modified electrodes were prepared upon addition of each component to NF which formed PEDOT:PSS@NF, $MgCoO_2$@NF, and $MgCoO_2$/PEDOT:PSS@NF. These electrodes were compared for their electrocatalytic activity in dual-chambered microbial fuel cells (MFCs). Sewage wastewater was used as feed stock while exoelectrogenic microbes present in wastewater served to generate bioelectricity upon utilizing organic waste and glucose as an electron donor. The maximum power and current density values were found to be 494 mWm^{-2} and 900 $mA\,m^{-2}$ using $MgCoO_2$/PEDOT:PSS@NF anode. It was ~2.5 times higher than that of unmodified NF anode. Electrochemical impedance spectroscopy (EIS) analysis exhibited reduction in charge transfer resistance for $MgCoO_2$/PEDOT:PSS@NF anode (25.26 Ω) compared to the unmodified NF anode (61.34 Ω). Thus, with the enhanced electrocatalytic activity and biocompatibility, $MgCoO_2$/PEDOT:PSS@NF anode offered better stability and porosity for dense biofilm formation which helped in the efficient generation of bioelectricity.

1. Introduction

Over the past decade, microbial fuel cells (MFCs) have been recognized as a competent technology in the treatment of wastewater in terms of generating reusable irrigational/portable water and renewable energy such as bioelectricity [1]. At this pace of dual benefit, generation of electricity is catalyzed by the exoelectrogenic microorganisms adhering onto the anode in a MFC system where the waste organic matters are degraded or metabolized under anaerobic condition to form electrons, protons, and CO_2 [2]. At the cathode, protons and electron equivalents combine with oxygen to form water, which completes the charge balance. As they pass through an external circuit, electron equivalents released during oxidative microbial metabolism can be used to generate a useful electromotive force [3]. In this established mechanism of electron transfer, anode plays a significant role in adhering the oxidizing microbial cells onto it and in transferring produced electrons to cathode [4]. Albeit studies suggest an increase in MFCs magnitude power density up to

10,000 orders during the past years, an efficient extracellular electron transfer upon oxidation of chemical bonds between organic components by the exoelectrogenic microorganisms remains a challenge [5].

Since anode materials have significant role in MFCs, there are numerous studies on the development, modification, and designing of the anode materials in order to subside the challenges in the construction and operation of MFCs [6–9]. The most common materials used in the construction of anode involve carbon-based materials [10, 11], metal/metal oxides, and conducting polymers [12]. However, in the case of conventional materials starting from carbon-based materials such as carbon paper, fibers, sheets, and rods; graphite-based sheets, brushes, fibers, and cloth; metal/metal oxide-based materials involving Fe, Ag, Au, Al, Cu, Co, and CuO; and other conducting polymers such as polyaniline and polypyrrole have been found not efficient in MFCs [6, 13, 14]. The drawbacks laid by these materials have poor stability, low mechanical strength, lesser surface area, larger pore size, corrosiveness, poor biocompatibility, and high cost [15]. To overcome the above-mentioned drawbacks, there is a need to construct an anode that remains stable and offer large surface area for microbial cell adhesion, unclogged pores, better electron transfer, and efficient generation of bioelectricity.

One promising method is to improve the anode's surface properties, and also prepare nanomaterials with complex structures and use them as anodes [16]. Synthesis of modified and doped forms of carbon materials [17], metal/metal oxides, and conducting polymers either in individual or composite forms have been put forward by various researchers to improve the power density, stability, surface area, microbial adhesion, electron transport, biocompatibility, conductivity, corrosion resistance, and electrochemical performance [18] along with cost-effectiveness [4, 19, 20]. Beside this, recently 3D-nickel (Ni) foam has drawn attention in the construction of anode by being base substratum. Among other transitional metals, Ni has remarkable abundance in nature; in addition to that, Ni is less toxic and economically feasible for application on large scale [21–23]. Ni usually exists in +2, +3, and +4 valence states; however, stable valence state in most of the conditions tends to be Ni(II). Ni ions at high valence state (Ni(III) and Ni(IV)) are suggested to execute strong oxidizing properties especially in electrochemical oxidative degradation (EOD) of organic compounds [24]. This property of Ni extends the application of 3D-Ni foam porous network towards designing an anode that would in turn have good conductivity and provide large specific area for efficient EOD of organic matters.

In the present study, an effective anode for a MFC is designed based on the above EOD properties of nickel, where nickel foam serves as the base substratum and enhances the EOD of organic matters present in the wastewater. In order to further improve conductivity and electrochemical properties of the anode, nickel foam was modified with a magnesium cobalt oxide ($MgCoO_2$) and poly(3,4-ethylenedioxythiophene) polystyrene sulfonate (PEDOT:PSS). As that of Ni, $Mg(OH)_2$ is also abundant in nature and has significant characteristics such as high negative standard potential (−2.3 vs. RHE), high melting point (649°C), low cost, and less toxic with an interesting electrochemical storage capacity [25], while PEDOT:PSS was reported to be a potential conducting polymer with influential characteristics such as high electrical conductivity, stability, durability, and ability to form thin homogenous layers [26]. Thus, this study investigated the fabrication of $MgCoO_2$/PEDOT:PSS@ nickel foam anode to set up simple, efficient, biocompatible, and cost-effective MFC with the capability of generating bioelectricity using sewage wastewater as feedstock (Scheme 1).

2. Experimental

2.1. Chemicals and Reagents. Magnesium sulphate heptahydrate ($MgSO_4{\cdot}7H_2O$) (99%) was purchased from Thermo Fisher Scientific, India. Cobalt (II) nitrate hexahydrate ($Co(NO_3)_2{\cdot}6H_2O$) (99%), 3,4-ethylenedioxythiophene (EDOT) (97%), poly(sodium 4-styrene sulfonate) (PSS) (Mw ~70,000), and N-Cetyl-N,N,N-Trimethyl Ammonium Bromide (CTAB) (98%) were acquired from Sigma-Aldrich, India. Sodium dihydrogen phosphate monohydrate ($H_2NaPO_4{\cdot}H_2O$) and sodium phosphate dibasic heptahydrate ($Na_2HPO_4{\cdot}7H_2O$) were obtained from Spectrochem Pvt. Ltd., India. Dextrose anhydrous was purchased from Loba Chemie, India. Ammonium persulphate ($(NH_4)_2S_2O_8$) (98%) and hydrochloric acid (HCl) were purchased from Finar Limited, India. Dimethyl sulfoxide (DMSO) was acquired from Sisco Research Laboratories Pvt. Ltd., India. Without further purifications, all of the chemicals were used as received.

2.2. Instrumentation. The Fourier transform infrared spectrometer from Shimadzu, IRTracer-100, was used to analyse the functional groups of the samples using the attenuated total reflectance (ATR) technique. CuKα radiation of wavelength ($X = 1.5406$) was utilised in the X'Pert Pro high-resolution X-ray diffractometer from BRUKER, USA, D8 Advance, Davinci, to perform the X-ray diffraction scans in the 2 theta range of 20°-80°. A Thermo Scientific Apreo S was utilised to analyse the morphological and microstructures of the samples ($MgCoO_2$, PEDOT:PSS, $MgCoO_2$/PEDOT:PSS composite, nickel foam, and microbial growth on the anode surface) using a high-resolution scanning electron microscopy (HR-SEM).

2.3. Preparation of the $MgCoO_2$. Synthesis of magnesium cobalt oxide ($MgCoO_2$) was carried out in a cost-effective manner by a sol-gel synthesis process as described by Maitra et al. [19]. Briefly, 0.5 M MgO and 0.12 M $Co(NO_3)_2{\cdot}6H_2O$ were used to prepare 50 mL of the reaction mixture to which triethanolamine ($C_6H_{15}NO_3$) was added dropwise as a chelating agent until the solution turned to pale pink. This was followed by agitating the reaction mixture at 150°C for 12 h or until the solution formed gel. Later, the formed gel was dried for 12 h at 60°C, powdered coarsely, and calcinated for 6 h at 850°C. The possible mechanism behind this sol-gel process was, initially, MgO dissociated to Mg^{+2} ions while dissolving in HNO_3^- and $Co(NO_3)_2{\cdot}6H_2O$ dissociated to Co^{+2} and NO_3^- ions while dissolving in H_2O. Next, agitation

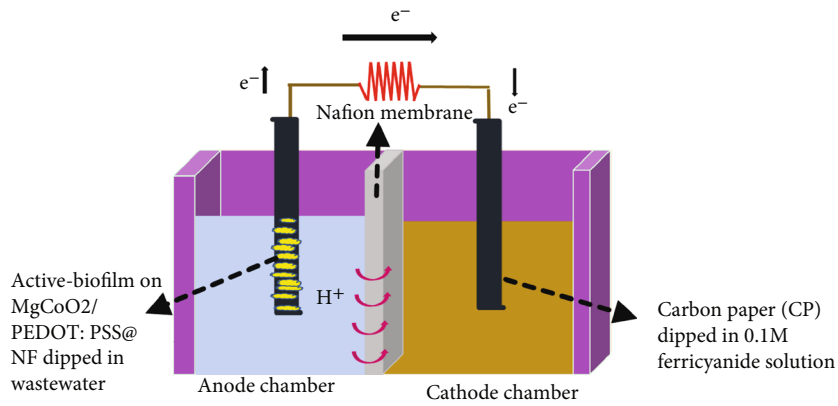

Scheme 1: Schematic representation of microbial fuel cell (MFC) set up to generate bioelectricity from sewage water.

at 150°C in the presence of $C_6H_{15}NO_3$ yielded hydrolysed forms of $C_6H_{15}NO_3^-$ radicals, in addition to Mg^{+2}, Co^{+2}, and H^+ ions. At this condition, several $C_6H_{15}NO_3^-$ radicals along with metal ions formed oligomeric clusters gradually resulting in a gel formation. Following this, drying and calcination processes evaporated the organic fractions present in the gel to form small $MgCoO_2$ crystallites that continuously nucleates to form larger grains.

2.4. Preparation of the PEDOT:PSS. PEDOT:PSS was prepared as per the method described by Ghosh et al. [27] with few modifications. Initially, 50 mL of the solution was prepared using 0.5 M aqueous HCl and 0.05 M CTAB to which 0.15 M ammonium persulphate ($(NH_4)_2S_2O_8$) was added dropwise. To this reaction mixture, 0.05 mM PSS was added followed by the addition of 0.15 M EDOT monomer. The reaction was carried out for 24 h at 60°C. During this reaction, $(NH_4)_2S_2O_8$ dissociates to form NH_4^+ and $S_2O_8^{2-}$ ions that homogenously disintegrates along with sulphate radicals oxidizing EDOT monomers to EDOT cations. The dopant PSSs are also reacted with EDOT during the polymerization process to form a dark blue PEDOT:PSS which is collected and washed with DI water to remove the unreacted monomers or ions. Later, the resulted PEDOT:PSS was dried for 24 h in a vacuum oven at 80°C.

2.5. Preparation of $MgCoO_2$/PEDOT:PSS Composite. 25 mg of $MgCoO_2$ was dispersed in a 5% PSS aqueous solution. Then, the mixture was kept stirring using a magnetic stirrer for 30 min and ultra-probe sonicated for 30 min. To prevent the oxidation via the dissolved oxygen, nitrogen gas (99.999%) was purged into the mixture for 30 min. Subsequently, 0.15 M EDOT monomer was added and again stirred for 24 h at ambient temperature. It resulted in a black colored $MgCoO_2$/PEDOT:PSS composite which was collected and washed with DI water to remove the unreacted monomers or ions. Finally, the $MgCoO_2$/PEDOT:PSS composite was dried in a vacuum oven at 80°C for 24 h.

2.6. Fabrication of Anode and Cathodes. To prepare the anode, nickel foam (NF) was cut into 1 cm × 5 cm pieces. Then, the NF pieces were subsequently treated with ethanol (99.99%), acetone (99.99%), and distilled water in a bath along with sonication, each phase lasting for 30 min. Pretreated NF electrodes were oven dried at 80°C for overnight. After that, each NF was coated with $MgCoO_2$, PEDOT:PSS, and $MgCoO_2$/PEDOT:PSS composite dispersions, which resulted in $MgCoO_2$, PEDOT:PSS, and $MgCoO_2$/PEDOT:PSS@Nickel foam anodes for MFC. Following this, cathode was prepared using a carbon paper (CP) which was also cut into 1 cm × 5 cm pieces. Similar to the above steps, CP pieces were consequently treated with ethanol (99.99%), acetone (99.99%), and distilled water in a bath sonication, each phase lasting for 30 min. Finally, the obtained CP electrodes were oven dried for overnight at 60°C and used as cathode in MFC. To prepare dispersions, 5% DMSO was used to disperse each individual and composite materials.

2.7. Inoculum Preparation. In the present study, wastewater was collected from a nearby lake at SRM Institute of Science and Technology, Kattankulathur, Tamil Nadu, India. After the collection of wastewater, it was kept undisturbed to obtain sludge sediment, later stored at 4°C for further analysis. The pH (10.5) and conductivity (2230 μS/cm) of the obtained wastewater were measured. In addition to the above prepared cost-effective anode, the use of wastewater sludge as an inoculum in bioelectricity generation makes the process more simple, feasible, and environmentally friendly approach. This method offered exoelectrogenic bacterial cultures in an inexpensive manner for the development of high-performance MFC [28].

2.8. Construction of MFC System and Measurements. Plexiglas chambered beakers were used to construct dual MFC chamber with a working volume of 100 mL each. Nafion 117 membrane (DuPont™ Nafion®) served as proton exchange membrane which was initially treated with distilled water at 80-90°C, followed by 5% H_2O_2 and 0.5 M H_2SO_4 for 1 h at 70-80°C. Later, the pretreated membrane was washed with distilled water and stored. Before installation and addition of inoculum to the anodic chamber, completely MFC system was sterilised. Experiments were carried out at room temperature (25±2°C); throughout the experiment, anaerobic condition was maintained in the

anode chamber while aerobic condition at the cathodic chamber. In the anodic chamber, sewage sludge was inoculated along with 55 mM glucose as the electron donor. Ferricyanide solution (50 mM) in 0.1 M PBS (pH 7) was used as catholyte. Electrochemical workstation with three-electrode cells (CHI-760E, CH Instrument, USA) was used to perform all of the electrochemical measurements such as cyclic voltammetry (CV) and electrochemical impedance spectroscopy (EIS). $MgCoO_2$/PEDOT:PSS@NF and CP were used as anode and cathode, respectively. Ag/AgCl (3 M KCl) and platinum wire served as reference and counter electrodes.

Energy generated by MFCs was calculated using polarization calculations and varied external loads. Following the power output stabilization, polarization and power density curves were generated by changing the external resistance (from 10 to 465 kΩ) applied to the circuit.

$$I = \frac{V}{R}, \tag{1}$$

where I represents the current, V represents the anticipated voltage, and R represents the applied resistance used to compute the current, while the formula $P = IV$ was used to calculate the power density. Anode surface area used to standardise the current and power densities [29].

3. Results and Discussion

3.1. Characterization of $MgCoO_2$/PEDOT:PSS@NF Electrode. The band energy red shifted due to the p-d exchange by the interaction between the localised d-electrons of Co^{2+} ions with that of Mg^{2+} cations. At the Fermi level of the valence band (VB), strong p-d (CoO) hybridization led to the VB maxima to migrate higher, which resulted in band gap bending. When Co is integrated into the MgO host lattice, the absorbance of MgO rises (up to its solubility limit). As a result, the enhanced UV emission intensity and redshift observed, both indicated that Co^{2+} ions are occupied the Mg^{2+} site in the MgO host lattice (data not shown) [30, 31]. Fourier transform infrared (FT-IR) spectroscopic analysis revealed the extent of EDOT polymerization in the presence of PSS and the incorporation of $MgCoO_2$ into the formed PEDOT:PSS nanocomposite matrix (Figure 1(c)). Synthesised PEDOT exhibited IR bands at 1360, 1433, and 1480 cm^{-1} due to C-C and C=C stretching of the quinoidal structure of the thiophene ring. Additional vibrational bands observed at 1244, 1141, and 1068 cm^{-1} corresponded to the ethylene oxide, and C-O-C bond stretching were observed (Figure 1(b)). PEDOT:PSS was also exhibited C-S bonds due to thiophene ring bands at 940, 902, and 826 cm^{-1}. In Figure 1(a), peaks at 1120, 1360, and 1630 cm^{-1} are ascribed to the presence of sulfonic acid group of PSS, C-C, and C=C bonds of the thiophene ring, respectively. Characteristic IR band of MgO bond vibration was observed at 510 cm^{-1}, while O-H due to surface water molecules and CoO in polymer matrix showed bands at 3429 and 421 cm^{-1}, respectively [19, 32, 33] (Figure 1(a)).

XRD spectra were further used to characterize the synthesised PEDOT:PSS, $MgCoO_2$, and $MgCoO_2$/PEDOT:PSS

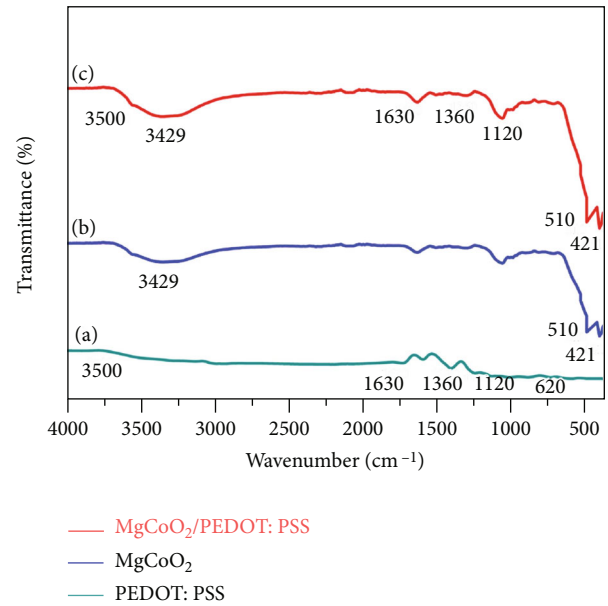

Figure 1: FT-IR spectra of (A) $MgCoO_2$, (B) PEDOT:PSS, and (C) $MgCoO_2$/PEDOT:PSS composite.

nanocomposite samples (Figures 2(a)–2(c)). It was reported that PEDOT:PSS has four characteristic peaks at 2θ of 3.7° and 6.6° attributed to low diffraction while bands at 17.7° and 26.0° were attributed to high diffraction which in turn reflects the lamella stacking and interchain stacking of PEDOT:PSS, respectively [34]. However, it also suggested that all polymers have the characteristic peak at 2θ of 26.0° which is related to interchain planar ring stacking [35]. In agreement to this statement, in the present study, PEDOT:PSS had revealed the peak at 2θ of 26.0°. In the case of $MgCoO_2$, the diffraction peaks found at 2θ of 36.79°, 44.79°, 64.21°, 74.31°, and 77.79°, corresponded to (111), (200), (220), (311), and (222) planes, respectively, which were found to match with the standard card number (JCPDS card no: 04-002-2875). However, in the case of PEDOT:PSS/$MgCoO_2$ composite, additional characteristic peak of PEDOT:PSS at 2θ of 26.0° was confirmed with the binding of $MgCoO_2$ into the polymer matrix (Figure 2(a)).

To ascertain about the surface morphology of the materials, HR-SEM images of nickel foam, $MgCoO_2$, PEDOT:PSS, and $MgCoO_2$/PEDOT:PSS composite were recorded (Figure 3). HR-SEM image of nickel foam revealed the 3D structure of numerous pores in the size ranging between 200 and 500 mm (Figure 3(a)). This unique network of porous structure suggested the increase in contact area between the collector and active material which in turn shortening the diffusion and migration of electrolyte ions, resulting in improved electrochemical performance [36]. PEDOT:PSS polymer matrix was found to have nanorod-like structure with CTAB molecules aiding as surfactant (Figure 3(b)). After the sample calcinated, $MgCoO_2$ was found to be in irregular globular form (Figure 3(c)). Finally, HR-SEM image of $MgCoO_2$/PEDOT:PSS composite confirmed the presence of irregular-globular $MgCoO_2$ coated onto PEDOT:PSS nanorods (Figure 3(d)).

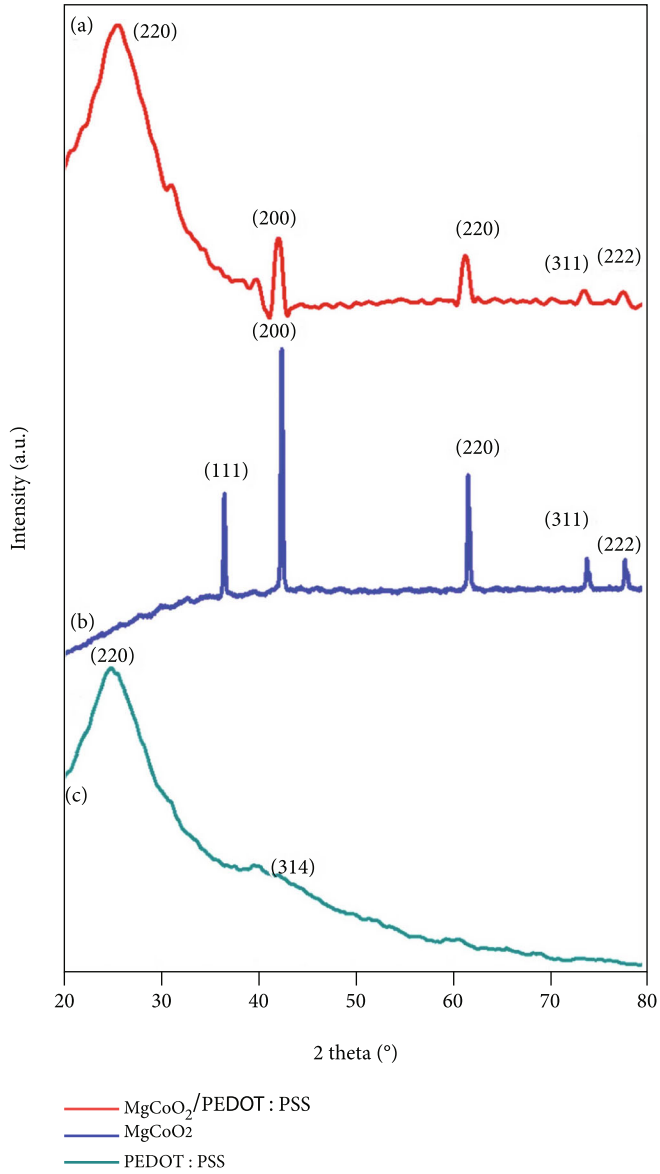

Figure 2: XRD spectra of (A) $MgCoO_2$/PEDOT:PSS, (B) $MgCoO_2$, and (C) PEDOT:PSS composite.

Furthermore, morphological characterizations of PEDOT:PSS@NF, $MgCoO_2$@NF, and $MgCoO_2$/PEDOT:PSS@NF composite were carried out after they have been used in MFCs system for ten days (Figure 4). Comparison of pretreated NF electrode surface before and after installation into a MFC system revealed the biofilm formation upon utilization of organic waste present in the wastewater by the microorganisms (Figure 4(a)). Biofilm formation was also observed on both the PEDOT:PSS@NF and $MgCoO_2$@NF matrix surfaces (Figures 4(a) and 4(b)). However, microbial population adhering onto $MgCoO_2$/PEDOT:PSS@NF composite was relatively high when compared to the above-mentioned individual matrixes (Figures 4(c) and 4(d)). This confirmed the biocompatibility of the $MgCoO_2$/PEDOT:PSS@NF anode for bioelectricity generation and wastewater treatment. This also revealed low cytotoxicity and biocompatibility of the fabricated anode which can be used in microbial cells.

3.2. Bioelectricity Generation. Electrode potentials, polarization curves, and power density were studied at each external resistance throughout the stabilization phase to assess the performance of anodic materials such as PEDOT:PSS@NF, $MgCoO_2$@NF, and $MgCoO_2$/PEDOT:PSS@NF in MFCs. Operation of MFC in the presence of $MgCoO_2$/PEDOT:PSS@NF as anode revealed that 85 h was required to reach a steady voltage output. Meanwhile, this time interval was sufficient for the microbial inoculum to multiply and form highly dense biofilm onto the anode surface. MFC installed with $MgCoO_2$/PEDOT:PSS@NF anode generated a stable voltage output of 0.9 V (Figure 5(a)). At the end of each cycle, utilized medium was replaced with the fresh growth medium, i.e., sewage wastewater. In the present study, electrocatalytic behaviour of $MgCoO_2$/PEDOT:PSS@NF anode towards glucose oxidation with increased long-term stability was found to be appealing with potential applications.

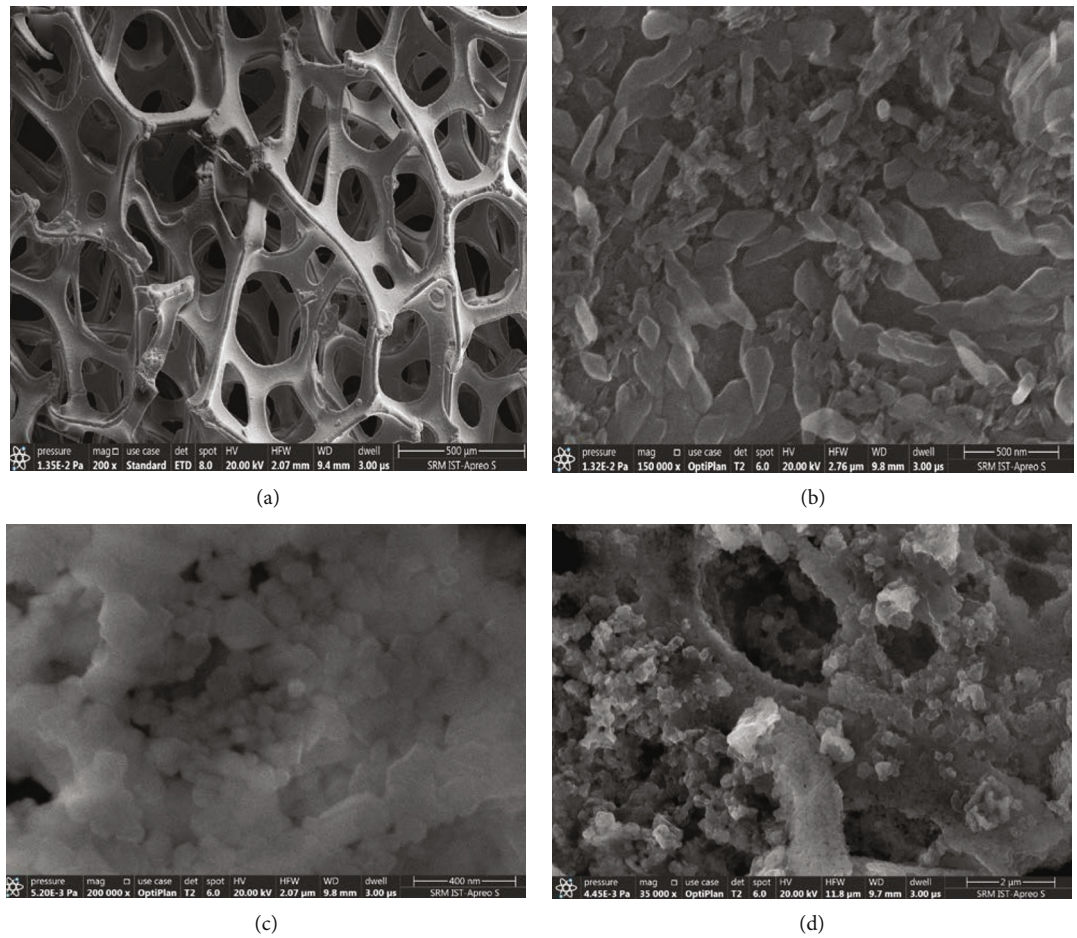

Figure 3: HR-SEM images of (a) NF, (b) PEDOT:PSS, (c) $MgCoO_2$, and (d) $MgCoO_2$/PEDOT:PSS composite.

Polarization and power density curves were evaluated when the voltage output remained constant to better understand the efficiency of the MFC. The changes in the external resistance were used to test the system, and the polarization and power density curves were extracted. In terms of the highest power density (494 mW/m^2) and current density (~900 mW/m^2), $MgCoO_2$/PEDOT:PSS@NF anode's performance was found to have been high (Figure 5(b)). Thus, the nickel-foam-based $MgCoO_2$/PEDOT:PSS anode was revealed to have high specific surface area that in turn reduces charge transfer resistance (R_{ct}) and allowed better electron transport between the biofilm and anode surface.

3.3. Electrochemical Performance. Anodes such as $MgCoO_2$/PEDOT:PSS@NF, $MgCoO_2$@NF, PEDOT:PSS@NF, and NF individually showed enhanced CV anodic peak currents in the potential ranging from -1 to 0.6 V. In terms of morphological characteristics such as porosity, physical and chemical stability, biocompatibility, large surface area, and efficient transport of electrons in the cathodic cell, $MgCoO_2$/PEDOT:PSS@NF is one of the best anodes that can be used to boost anodic peak current with high performance. It is suggested that as there is an increase in voltage scan rate, the interaction between the metallic oxide and conducting polymer could improve the activity of the electrodes. Since anode plays a significant role in electron transport, the decrease in overpotential could be associated with acceleration of electron supply to cathode or due to enhanced electron transfer kinetics from exoelectrogeneic microbes to anode [37]. Cyclic voltammetry (CV) analysis of NF, PEDOT:PSS@NF, $MgCoO_2$@NF, and $MgCoO_2$/PEDOT:PSS@NF was performed at a scan rate of 50 mVs^{-1} to further understand the bioelectrocatalytic behaviour towards anodic biofilms and electron transfer mechanism towards cathode. Both the anodic and cathodic peaks indicated that the MFCs contained dissolved redox species which are hypothesized to serve as electron transporters [38]. From the CV curves, it is evidenced that $MgCoO_2$/PEDOT:PSS@NF showed a higher anodic limiting current density (2.1 mA) which was nearly three times higher than the current obtained using unmodified NF (0.8 mA) (Figure 6). On the other hand, bare NF anode electrode exhibited wide rectangular CV curve which revealed a potential electrochemical double layer capacitive behaviour in comparison with $MgCoO_2$/PEDOT:PSS composite. This suggested that the efficiency of additional anodic components such as metal oxides and conducting polymers could improve the surface area and charge potential.

3.4. Evaluation of Electrocatalytic Activity of Fabricated Anode. Electrocatalytic activity of the $MgCoO_2$/PEDOT:PSS@NF electrode was evaluated by electrochemical

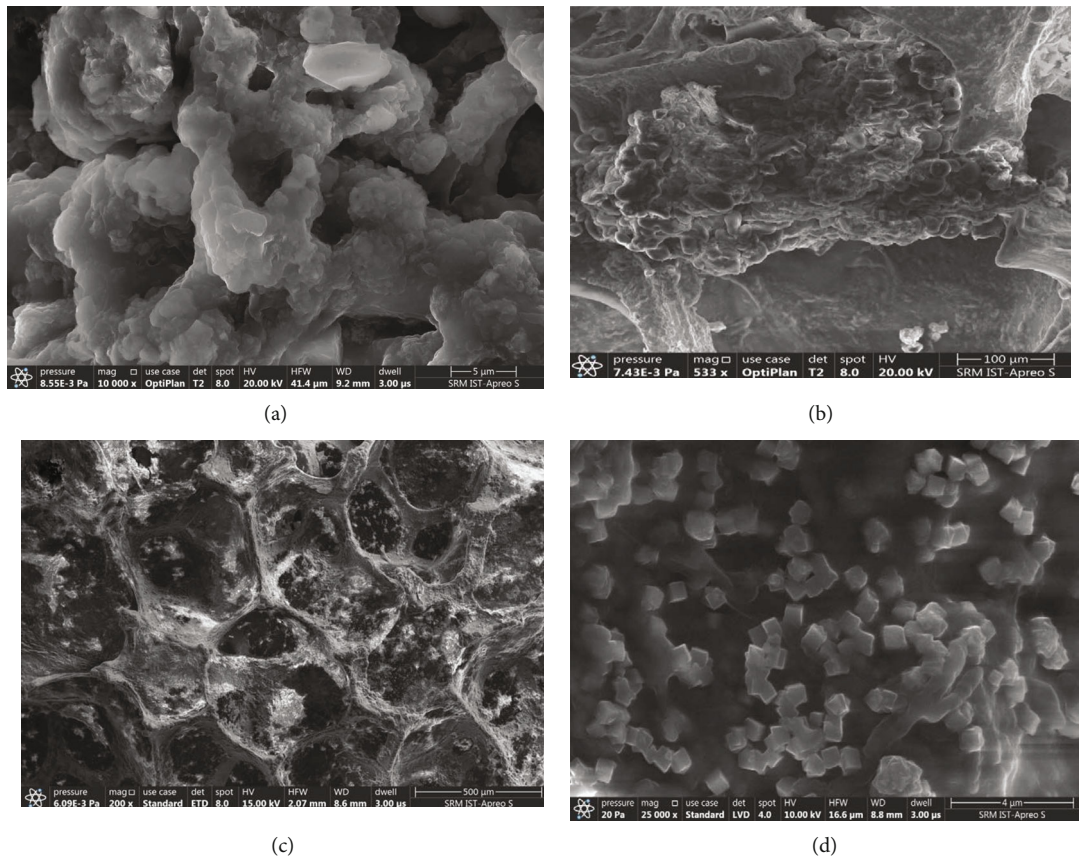

Figure 4: HR-SEM images of biofilm formed onto (a) PEDOT:PSS@NF, (b) $MgCoO_2$@NF, and (c, d) $MgCoO_2$/PEDOT:PSS@NF.

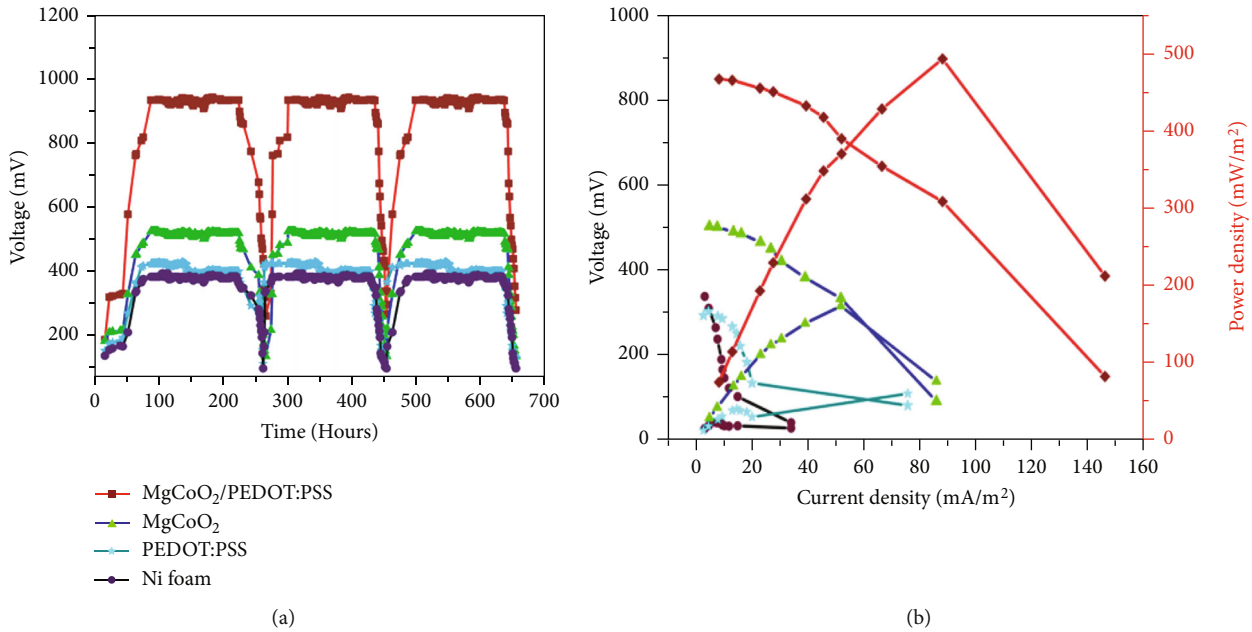

Figure 5: (a) Electricity generated using a dual-chambered MFC and (b) current and power densities generated while functioning MFC system in the presence of sewage wastewater using NF (black color), PEDOT:PSS@NF (green color), $MgCoO_2$@NF (blue color), and $MgCoO_2$/PEDOT:PSS@NF (red color) as anodes.

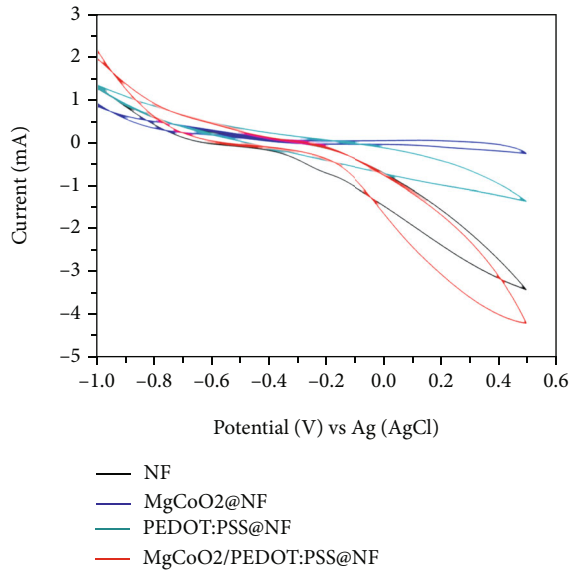

Figure 6: Cyclic voltammograms of the NF (black color), PEDOT:PSS@NF (green color), $MgCoO_2$@NF (blue color), and $MgCoO_2$/PEDOT:PSS @NF (red color) as anodes in a MFC system at a scan rate of 50 mV/s.

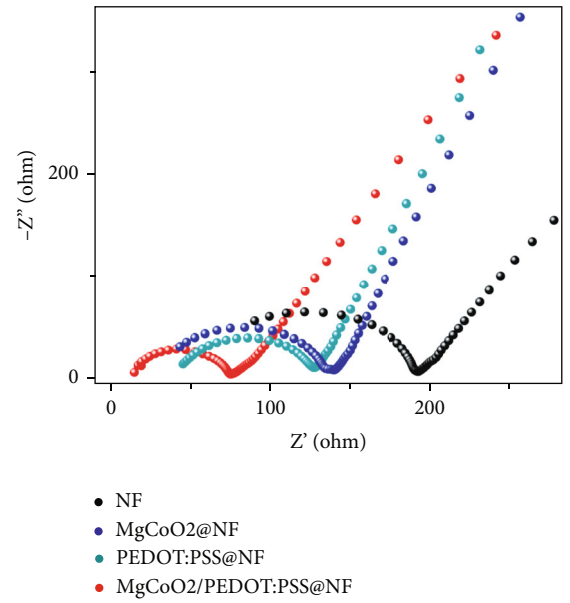

Figure 7: The Nyquist curves were recorded for NF (black color), PEDOT:PSS@NF (green color), $MgCoO_2$@NF (blue color), and $MgCoO_2$/PEDOT:PSS @NF (red color) as anodes in MFCs.

impedance spectroscopy (EIS) using a typical three-cell electrode apparatus (Figure 7). In general, charge transfer resistance (R_{ct}) of the working electrode is related to the diameter of semicircle which can indicate the interfacial processes of charge transport between the electrode surface and electrolyte ions [38]. In the study, EIS plots are represented by straight lines at lower frequency range whereas semicircles at higher frequency range [39]. The semicircle is formed due to charge transfer and capacitive resistance, while straight line indicates the diffusion resistance characterized by Warburg mass transfer resistance [40]. The internal resistance including polarization resistance of the cathode, ohmic resistance, and double layer capacitance were accounted to be constant [41]. $MgCoO_2$/PEDOT:PSS@NF anode (25.26 Ω) exhibited the shortest semicircle with the low charge transfer resistance when compared to the $MgCoO_2$@NF (39.09 Ω), PEDOT:PSS@NF (55.78 Ω), and NF anode (61.34 Ω) (Figure 7). The decrease in R_{ct} value indicated the higher electroactivity of the $MgCoO_2$/PEDOT:PSS@NF anode which was directly related to an improved adherence of microbial cells (biofilm formation) onto the electrode compared to that NF anode.

4. Conclusion

In summary, we have demonstrated an anode material using nickel foam modified with $MgCoO_2$ and PEDOT:PSS that had significantly improved porosity, biocompatibility, and conductivity. When compared to unmodified NF, $MgCoO_2$/PEDOT:PSS nanocomposite-coated NF had great influence on the adhesion of microbial cells which may be due to the large surface area offered by irregular globular structures of calcinated $MgCoO_2$. The dense biofilm formed in combination with PEDOT:PSS had improved the anodic reaction, in turn transferring electrons to the cathodic chamber in an efficient manner. Thus, the $MgCoO_2$/PEDOT:PSS-based anode developed in the present study can be used to setup MFC to generate bioelectricity at a lower cost. This new anode material has to be further studied in order to implement at large scale in combination with wastewater treatment system to produce bioelectricity.

Data Availability

Data will be provided upon request.

Conflicts of Interest

The authors declare that they have no conflicts of interest.

Authors' Contributions

Brahmari H. Shetty and Raji Atchudan contributed equally in this study.

Acknowledgments

We sincerely thank the Department of Science and Technology (DST) (International Bilateral Cooperation Division), India, for the financial support through "INDO-RUSSIA Project" (File No. INT/RUS/RFBR/385). AKS thanks the Science and Engineering Research Board for the funded project (File No. CRG/2021/001517). We also acknowledge the SRM-IST for supporting "high-resolution scanning electron microscope (HR-SEM) and micro-Raman facility". BHS thanks the Department of Science and Technology (DST) for the fellowship provided in the form of project assistantship. This work was funded by the Researchers Supporting

Project Number (RSP-2021/243), King Saud University, Riyadh, Saudi Arabia.

References

[1] R. Jerome, B. Shetty, D. Ganapathy et al., "Thermally expanded graphite incorporated with PEDOT:PSS based anode for microbial fuel cells with high bioelectricity production," *Journal of The Electrochemical Society*, vol. 169, article 017515, 2022.

[2] B. Bian, C. Wang, M. Hu et al., "Application of 3D printed porous copper anode in microbial fuel cells," *Frontiers in Energy Research*, vol. 6, p. 50, 2018.

[3] V. B. Wang, J. Du, X. Chen et al., "Improving charge collection in Escherichia coli–carbon electrode devices with conjugated oligoelectrolytes," *Physical Chemistry Chemical Physics*, vol. 15, no. 16, pp. 5867–5872, 2013.

[4] F. Nourbakhsh, M. Mohsennia, and M. Pazouki, "Nickel oxide/carbon nanotube/polyaniline nanocomposite as bifunctional anode catalyst for high-performance Shewanella-based dual-chamber microbial fuel cell," *Bioprocess and Biosystems Engineering*, vol. 40, no. 11, pp. 1669–1677, 2017.

[5] F. A. Alatraktchi, Y. Zhang, and I. Angelidaki, "Nanomodification of the electrodes in microbial fuel cell: impact of nanoparticle density on electricity production and microbial community," *Applied Energy*, vol. 116, pp. 216–222, 2014.

[6] A. A. Yaqoob, M. N. M. Ibrahim, and S. Rodríguez-Couto, "Development and modification of materials to build cost-effective anodes for microbial fuel cells (MFCs): an overview," *Biochemical Engineering Journal*, vol. 164, p. 107779, 2020.

[7] X. Peng, X. Chu, S. Wang, K. Shan, D. Song, and Y. Zhou, "Bio-power performance enhancement in microbial fuel cell using Ni-ferrite decorated anode," *RSC Advances*, vol. 7, no. 26, pp. 16027–16032, 2017.

[8] A. Singh and A. Kaushik, "Removal of Cd and Ni with enhanced energy generation using biocathode microbial fuel cell: insights from molecular characterization of biofilm communities," *Journal of Cleaner Production*, vol. 315, p. 127940, 2021.

[9] I. Gajda, J. Greenman, and I. A. Ieropoulos, "Recent advancements in real-world microbial fuel cell applications," *Current Opinion in Electrochemistry*, vol. 11, pp. 78–83, 2018.

[10] P. Murugan, R. D. Nagarajan, B. H. Shetty, M. Govindasamy, and A. K. Sundramoorthy, "Recent trends in the applications of thermally expanded graphite for energy storage and sensors – a review," *Nanoscale Advances*, vol. 3, no. 22, pp. 6294–6309, 2021.

[11] V. Magesh, A. K. Sundramoorthy, and D. Ganapathy, "Recent advances on synthesis and potential applications of carbon quantum dots," *Frontiers in Materials*, vol. 9, article 906838, 2022.

[12] G. G. Kumar, V. G. S. Sarathi, and K. S. Nahm, "Recent advances and challenges in the anode architecture and their modifications for the applications of microbial fuel cells," *Biosensors and Bioelectronics*, vol. 43, pp. 461–475, 2013.

[13] R. Nitisoravut, C. N. D. Thanh, and R. Regmi, "Microbial fuel cells: advances in electrode modifications for improvement of system performance," *International Journal of Green Energy*, vol. 14, no. 8, pp. 712–723, 2017.

[14] M. Rahimnejad, A. Adhami, S. Darvari, A. Zirepour, and S.-E. Oh, "Microbial fuel cell as new technology for bioelectricity generation: a review," *Alexandria Engineering Journal*, vol. 54, no. 3, pp. 745–756, 2015.

[15] J. M. Sonawane, S. A. Patil, P. C. Ghosh, and S. B. Adeloju, "Low-cost stainless-steel wool anodes modified with polyaniline and polypyrrole for high-performance microbial fuel cells," *Journal of Power Sources*, vol. 379, pp. 103–114, 2018.

[16] R. B. Song, Y. C. Wu, Z. Q. Lin et al., "Living and conducting: coating individual bacterial cells with in situ formed polypyrrole," *Angewandte Chemie - International Edition*, vol. 56, no. 35, pp. 10516–10520, 2017.

[17] X. Fan, Y. Zhou, X. Jin, R. B. Song, Z. Li, and Q. Zhang, "Carbon material-based anodes in the microbial fuel cells," *Carbon Energy*, vol. 3, no. 3, pp. 449–472, 2021.

[18] A. K. Sundramoorthy and S. Gunasekaran, "Applications of graphene in quality assurance and safety of food," *TrAC Trends in Analytical Chemistry*, vol. 60, pp. 36–53, 2014.

[19] S. Maitra, P. K. Chakraborty, R. Mitra, and T. K. Nath, "Electrochemical aspects of sol-gel synthesized $MgCoO_2$ for aqueous supercapacitor and alkaline HER electrocatalyst applications," *Current Applied Physics*, vol. 20, no. 12, pp. 1404–1415, 2020.

[20] S. You, M. Ma, W. Wang et al., "3D macroporous nitrogen-enriched graphitic carbon scaffold for efficient bioelectricity generation in microbial fuel cells," *Advanced Energy Materials*, vol. 7, no. 4, p. 1601364, 2017.

[21] G.-F. Chen, T. Y. Ma, Z.-Q. Liu et al., "Efficient and stable bifunctional electrocatalysts Ni/NixMy (M = P, S) for overall water splitting," *Advanced Functional Materials*, vol. 26, no. 19, pp. 3314–3323, 2016.

[22] W. Zhu, X. Yue, W. Zhang et al., "Nickel sulfide microsphere film on Ni foam as an efficient bifunctional electrocatalyst for overall water splitting," *Chemical Communications*, vol. 52, no. 7, pp. 1486–1489, 2016.

[23] Y. Miao, L. Ouyang, S. Zhou et al., "Electrocatalysis and electroanalysis of nickel, its oxides, hydroxides and oxyhydroxides toward small molecules," *Biosensors and Bioelectronics*, vol. 53, pp. 428–439, 2014.

[24] S. Sun, P. Diao, C. Feng et al., "Nickel-foam-supported β-Ni(OH)2as a green anodic catalyst for energy efficient electro-oxidative degradation of azo-dye wastewater," *RSC Advances*, vol. 8, no. 35, pp. 19776–19785, 2018.

[25] A. Nanwani, K. A. Deshmukh, P. Sivaraman et al., "Two-dimensional layered magnesium-cobalt hydroxide crochet structure for high rate and long stable supercapacitor application," *NPJ 2D Materials and Applications*, vol. 3, no. 1, pp. 1–7, 2019.

[26] Y. Wang, S. Li, J. Sun, Y. Zhang, H. Chen, and C. Xu, "Simple solvothermal synthesis of magnesium cobaltite microflowers as a battery grade material with high electrochemical performances," *Ceramics International*, vol. 45, no. 12, pp. 14642–14651, 2019.

[27] S. Ghosh, A. K. Mallik, and R. N. Basu, "Enhanced photocatalytic activity and photoresponse of poly(3,4-ethylenedioxythiophene) nanofibers decorated with gold nanoparticle under visible light," *Solar Energy*, vol. 159, pp. 548–560, 2018.

[28] F. Zhang, Z. Ge, J. Grimaud, J. Hurst, and Z. He, "Long-term performance of liter-scale microbial fuel cells treating primary effluent installed in a municipal wastewater treatment facility," *Environmental Science & Technology*, vol. 47, no. 9, pp. 4941–4948, 2013.

[29] B. Thulasinathan, J. O. Ebenezer, A. Bora et al., "Bioelectricity generation and analysis of anode biofilm metabolites from

septic tank wastewater in microbial fuel cells," *International Journal of Energy Research*, vol. 45, no. 12, pp. 17244–17258, 2021.

[30] M. R. Bindhu, M. Umadevi, M. Kavin Micheal, M. V. Arasu, and N. Abdullah Al-Dhabi, "Structural, morphological and optical properties of MgO nanoparticles for antibacterial applications," *Materials Letters*, vol. 166, pp. 19–22, 2016.

[31] M. M. Obeid, S. J. Edrees, and M. M. Shukur, "Synthesis and characterization of pure and cobalt doped magnesium oxide nanoparticles: insight from experimental and theoretical investigation," *Superlattices and Microstructures*, vol. 122, pp. 124–139, 2018.

[32] A. K. Sundramoorthy, B. S. Premkumar, and S. Gunasekaran, "Reduced graphene oxide-poly(3,4-ethylenedioxythiophene) polystyrenesulfonate based dual-selective sensor for iron in different oxidation states," *ACS Sensors*, vol. 1, no. 2, pp. 151–157, 2016.

[33] N. G. Yasri, A. K. Sundramoorthy, W.-J. Chang, and S. Gunasekaran, "Highly selective mercury detection at partially oxidized graphene/poly(3,4-ethylenedioxythiophene):-poly(styrenesulfonate) nanocomposite film-modified electrode," *Frontiers in Materials*, vol. 1, p. 33, 2014.

[34] N. Kim, S. Kee, S. H. Lee et al., "Highly conductive PEDOT:PSS nanofibrils induced by solution-processed crystallization," *Advanced Materials*, vol. 26, no. 14, pp. 2268–2272, 2014.

[35] Q. Zhao, R. Jamal, L. Zhang, M. Wang, and T. Abdiryim, "The structure and properties of PEDOT synthesized by template-free solution method," *Nanoscale Research Letters*, vol. 9, no. 1, p. 557, 2014.

[36] Z. Zhang, X. Liu, X. Qi, Z. Huang, L. Ren, and J. Zhong, "Hydrothermal synthesis of Ni3S2/graphene electrode and its application in a supercapacitor," *RSC Advances*, vol. 4, no. 70, pp. 37278–37283, 2014.

[37] R. Karthikeyan, N. Krishnaraj, A. Selvam et al., "Effect of composites based nickel foam anode in microbial fuel cell using Acetobacter aceti and Gluconobacter roseus as a biocatalysts," *Bioresource Technology*, vol. 217, pp. 113–120, 2016.

[38] H. Yuan, L. Deng, Y. Chen, and Y. Yuan, "MnO2/Polypyrrole/MnO2 multi-walled-nanotube-modified anode for high-performance microbial fuel cells," *Electrochimica Acta*, vol. 196, pp. 280–285, 2016.

[39] P. Murugan, A. K. Sundramoorthy, D. Ganapathy, R. Atchudan, D. Nallaswamy, and A. Khosla, "Electrochemical detection of H_2O_2 Using an activated glassy carbon electrode," *ECS Sensors Plus*, vol. 1, no. 3, article 034401, 2022.

[40] S. Singh, A. Pophali, R. A. Omar et al., "A nickel oxide-decorated *in situ* grown 3-D graphitic forest engrained carbon foam electrode for microbial fuel cells," *Chemical Communications*, vol. 57, no. 7, pp. 879–882, 2021.

[41] A. K. Manohar, O. Bretschger, K. H. Nealson, and F. Mansfeld, "The use of electrochemical impedance spectroscopy (EIS) in the evaluation of the electrochemical properties of a microbial fuel cell," *Bioelectrochemistry*, vol. 72, no. 2, pp. 149–154, 2008.